

Elimination of Methyl Orange Dye with Three Dimensional Electro-Fenton and Sono-Electro-Fenton Systems Utilizing Copper Foam and Activated Carbon

Zahraa M. Hameed¹, Rasha H. Salman^{1*}

¹ Department of Chemical Engineering, College of Engineering, University of Baghdad, Baghdad, Iraq

* Corresponding author e-mail: rasha.habeeb@coeng.uobaghdad.edu.iq

ABSTRACT

This study deals with the elimination of methyl orange (MO) from an aqueous solution by utilizing the 3D electro-Fenton process in a batch reactor with an anode of porous graphite and a cathode of copper foam in the presence of granular activated carbon (GAC) as a third pole, besides, employing response surface methodology (RSM) in combination with Box-Behnken Design (BBD) for studying the effects of operational conditions, such as current density (3–8 mA/cm²), electrolysis time (10–20 min), and the amount of GAC (1–3 g) on the removal efficiency beside to their interaction. The model was veiled since the value of R² was high (>0.98) and the current density had the greatest influence on the response. The best removal efficiency (MO Re%) at pH = 3 was 95.62% with an average energy consumption of 6.22 kWh/kg MO, which was achieved under maximal conditions of current density = 5.12 mA/cm², mass of GAC = 3 g, and time = 20 min with small amounts of Fe²⁺ (0.124 mM), and Na₂SO₄ (0.02 M). Moreover, the present work investigated the effectiveness of 3D electro-Fenton assisted by ultrasound known as Sono-Electro-Fenton (SEF), by following a new strategy based on applying the minimum circumstances of EF and comparing its results with that of SEF under the same conditions. MO Re% for EF_{min} was 49.24% while SEF was 50.51%, which is considered an exiguous improvement. However, using copper foam as a working electrode in the 3D EF system for the degradation of MO was an excellent choice. Furthermore, the suggested approach is characterized by simplicity, speed, and efficiency with a high percentage of pollutant removal, in addition to being eco-friendly.

Keywords: Cu foam, activated carbon, three dimensional, Electro-Fenton, Sono-Electro-Fenton.

INTRODUCTION

Water is considered an essential source for the survival of living organisms, and it is also a distinctive feature of planet Earth, as it plays a crucial role in all aspects of human life (Staddon, 2016). Due to the increase in population growth, climate change, and water exposure to many pollutants, the availability of usable water, as well as its quality, has become a global problem (Tetteh et al., 2020). One of the greatest challenges that the world faces at the present time is treating wastewater resulting from various industries. Huge amounts of water are consumed by industrial processes, and the water that is disposed of contains many different substances (Benmessaoud et al., 2022); one of

these effluents corresponds to synthetic dyes (Sala and Gutiérrez-Bouzán, 2014).

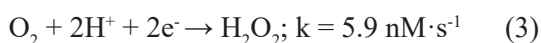
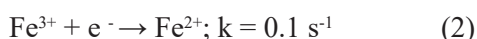
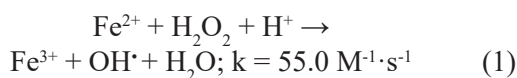
Azo dyes have been widely used in many fields in our lives, such as textiles, dyeing, cosmetics, and others. These dyes are among the most broadly used dyes, constituting more than 50% of the dyes used in industry. Due to their high toxicity, they cause serious problems that affect both aquatic and human life, such as cancer and mutagenic effects, besides their high chemical stability and versatility (Vainoris et al., 2022; Mohammed et al., 2023). Therefore, it has become imperative to treat wastewater containing these materials.

In the field of removing these dyes, several methods and strategies have been reported, such as membrane separation (Al-Bayati et al., 2023), coagulation-flocculation (Igwegbe et al., 2021),

filtration (Abed and Waisi, 2024), and biological (Najim and Mohammed, 2018). However, these techniques have many disadvantages like high operational cost, sludge removal, complexity, and caused damage to yeast and bacteria strains (Ganzenko et al., 2018).

Advanced oxidation technology, as a suitable alternative process, has been employed to remove these dyes in an efficient manner (Mohammed et al., 2020; Yerima et al., 2024), as it is characterized by low costs and does not require complex operating equipment (Jasim and Salman, 2024a), in addition to its ability to break down a lot of poisonous organic pollutants (Hameed and Mousa, 2019).

Electro-Fenton is one of the most efficient techniques of advanced oxidation processes (AOP), as it has been proven successful in removing many hazardous pollutants such as phenol (Abbas and Abbas, 2022), petroleum refinery (Fahem and Abbar, 2020), dyes (Rivera et al., 2022), etc. Electro-Fenton is built on the Fenton reaction, where hydroxyl radicals (OH^\bullet) are generated in situ through the reaction of iron ions with hydrogen peroxide (H_2O_2) as shown in Equation 1. This technology has many advantages, such as the possibility of regenerating ferrous ions through the reduction reaction on the cathode surface of the ferric ion as illustrated in Equation 2, and continuous electrolytic generation of hydrogen peroxide as shown in Equation 3 (Eslami et al., 2021).



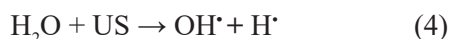
There are few studies which investigated the removal of MO with electro-Fenton process, such as Adachi et al. (Adachi et al., 2022) who obtained MO removal % of 94.5 within 60 min by utilizing graphite as cathode in the presence of $[\text{Fe}^{2+}] = 0.232 \text{ mM}$, $[\text{H}_2\text{O}_2] = 8.8 \text{ mM}$ and $[\text{Na}_2\text{SO}_4] = 0.05 \text{ M}$.

The high surface area of the electrodes is an important factor in raising the production of both Fe^{2+} and H_2O_2 (Fahem and Abbar, 2020). The enhancement of hydroxyl radicals generation can be achieved by increasing the electrode conductivity as well as its specific surface area, as a final result, the removal of contaminants is improved (Zhu et al., 2020). Because copper foam possesses the above-mentioned advantages, it was used as the working electrode (cathode) in the present study. To achieve a greater raising in the

specific surface area of the working electrode, the three-dimensional electrode technology is used by employing activated carbon granules as a third electrode (Sun et al., 2017). This technology has become interesting to many researchers, because it degrades organic materials with high efficiency, due to its ease of use and its great effectiveness, in addition to being environmentally friendly (Zhang et al., 2020). Furthermore, the 3D electrode technology has proven superior to the 2D electrode technology in terms of removing pollutants, energy consumption, and current efficiency (Zheng et al., 2019). When the Electro-Fenton reactor is supplied with granular activated carbon, it leads to minimization of the concentration polarization by forming several microelectrodes (Zhang et al., 2019). The effectiveness of removal would be enhanced because the space between the activated carbon particles is shorter, which allows the transfer of electrons faster (Yang and Tang, 2018). Also, granular activated carbon (GAC) provides a large active contact area, as a 3D pole system that makes the electrochemical reaction prolong to the external of each particle electrode in addition to the basic electrode that reacted initially (Thwaini and Salman, 2023). Granular electrodes are suitable to utilize as 3D electrodes, because they have remarkable conductivity, premium chemical stability as well as a large surface area (Norra and Radjenovic, 2021).

Recently, combining advanced oxidation techniques has been used to improve the single-function performance of these systems (Babunusami and Muthukumar, 2014; Ghjeer and Abbar, 2023). Ultrasonic irradiation is one of the advanced oxidation methods that lead to the decomposition of organic materials and its effect through cavitation, being the creation, outgrowth, and then collapse of the microbubbles, which generates high temperature and pressure and thus a thermal decomposition of water causing the generation of reactive OH^\bullet as predicted in Equation 4 (Hasani et al., 2020). However, using the sonolysis alone is not sufficient to achieve maximum dye removal (Giray et al., 2014). Therefore, ultrasonic wave irradiation is combined with electric Fenton to clean the electrodes and improve the rate of mass transfer of the ferrous ion and oxygen in the direction of the cathode to achieve reduction reactions to generate both the ferric ion and hydrogen peroxide needed to produce the oxidizing agent OH^\bullet through the Fenton reaction. Thus, reducing the energy consumed as well as the amount of OH^\bullet generated by acoustic

decomposition would be attained (Hasani et al., 2020; Dargahi et al., 2023).



The main goal of the present study was to investigate the enhancement of MO removal by utilizing Cu foam in a 3D Electro-Fenton system. To the best of authors' knowledge, no previous studies examined it up to now. Besides, attaining the optimal operating conditions for removing methyl orange, while demonstrating the effect of adding activated carbon granules and testing its performance as a third electrode to the electrical cell that consisting of copper foam as the cathode where a few studies utilized it as the working electrode besides porous graphite as the anode. In addition, the present study would test the effect of the combination between electrical Fenton and ultrasound on the removal efficiency.

EXPERIMENTAL WORK

Methods and materials

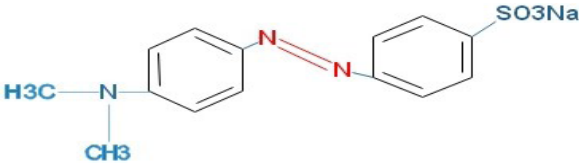
All materials used in this research are of high purity and did not require further purification. These chemicals were methyl orange powder (BDH, Company) as the basic organic pollutant and its physical properties and structure are illustrated in Table 1, ferrous sulfate heptahydrate (CDH, Company) as the source of ferrous ions, sodium sulfates (with 99.0% purity, SDFCL) as electrolyte, and 0.1 M of sulfuric acid (with 98% purity, Sigma-Aldrich) with 0.1 M of sodium hydroxide (98% purity, ORPITAL) which were utilized to obtain a pH equal to 3 in all experiments. GAC (Sigma-Aldrich). The aqueous solutions were prepared with deionized water.

Electrolytic system

A batch glass cell of 1 L containing 0.7 L of aqueous solution of methyl orange (MO) with concentration of 100 mg/L was used as the electrolytic cell. The reactor was covered by a Perspex cover of 10 mm thickness, with two slits for fixing the electrodes and three bores for introducing the airflow exporter, the thermometer, and the sample ejecting. Copper foam plate from Xiamen Top New Energy Technology (China) was employed as the cathode with dimensions 130×50×10 mm which had a porosity > 98% with pores per inch of 110, and porous graphite plate as the anode (130×50×5 mm) with a space of 3 cm between them. Copper foam was cleaned by using 10% of acetic acid to remove any oxide layers on its surface and then washed by deionized water. At the beginning, for 20 min and with a rate of 18 L/h air was bubbled into the solution by using an air compressor (model-ACO-208,55W, China) and persevered until the completion of the experiment. The air is spread into the solution using a glass tube equipped with a diffuser. To achieve the required current density, a power supply of 0–30 V and 0–5 A with model (UNI-T, UTP3315PE) was used. A 0.124 mM of ferrous sulfate heptahydrate was added for supplying the reaction with Fe⁺² and 0.02 M of Na₂SO₄ was used as supporting electrolyte. The best value of the pH for electro-Fenton systems was 3 (Thwaini and Salman, 2023) so to adjustment this value, 0.1 M of H₂SO₄ and 0.1 M of NaOH was utilized.

Before employing GAC as a third electrode, it was sieved into particles with diameters larger than 1.5 mm using a No. 16 (1.18 mm) sieve, followed by washing with deionized water to eliminate any impurities, and lastly dried in an oven for 6 hours at 105 °C (Roddaeng et

Table 1. The physical properties and structure of methyl orange dye

| | |
|----------------|--|
| Structure |  |
| Chemical name | 4-dimethylaminoazobenzene-4-sulfonic acid sodium |
| Molecular mass | 327.33 g/mol |
| Density | 0.791 g/cm ³ |
| Type of dye | Acidic azo dye |

al., 2018). The specific surface area and the pore size of GAC were measured by utilizing Brunauer-Emmett-Teller (BET) according to N_2 -adsorption/desorption isotherm at 77 K (Thermo finnigan, USA). GAC properties were a specific surface area of $1023 \text{ m}^2/\text{g}$ with $0.2924 \text{ cm}^3/\text{g}$ as pore size. At the start and end of each run, the samples were drawn and then centrifuged at 400 rpm for 15 minutes, and the concentration of MO was determined by (Spectrometers, UV-9200, UK) at wavelength (λ) of 464 nm. To accomplish the experiment of Sono-Electro-Fenton, the same electrolytic cell was utilized with submerging it into an ultrasonic bath at 40 KHz with 60 Watt (ISOLAB Laborgerger GmbH, Germany). Figure 1 shows a schematic diagram of the 3D Electro Fenton and the 3D Sono Electro Fenton systems. The MO elimination efficiency was determined by Equation 5, as follows (Hassan et al., 2022):

$$MO \text{ Re}\% = ((C_0 - C_f)/C_0) \times 100 \quad (5)$$

where: C_0 and C_f is the initial and the final concentration of MO (mg/L) respectively, $MO \text{ Re}\%$ is the MO removal efficiency.

To calculate the amount of energy consumed (EC) to decompose one kilogram of methyl orange,

Equation 6 was used for estimation the value of EC in kWh/kg MO (Jasim and Salman, 2024a).

$$EC = (I \times U \times t \times 1000)/(\Delta MO \times V_s) \quad (6)$$

where: U is the voltage (v), I is the applied current of the operation (Ampere), ΔMO is the MO degradation during the test (mg/L), t is the reaction time (h), and V_s is the volume of electrolytic solution (L).

Characterization of electrodes

Copper foam and porous graphite were utilized as cathode and anode, respectively. The electrodes structures were analyzed by utilizing an X-ray diffractometer (Shimadzu, XRD 6000 model, Japan). The source of X-ray was $\text{CuK}\alpha$ radiation and the X-ray tube was operated at current of 30 mA and voltage of 40 kV with scan speed of 5 degrees per minute. The XRD patterns of copper foam and porous graphite were described in Figure 2. The copper foam structure analysis exhibits 3 strong curving peaks at 43.298° with hkl of 111, 50.434° (200) and 74.133° (220) (Ma et al., 2021), while the XRD result of porous graphite displays a sharp peak at $2\theta = 26.382^\circ$, corresponding to line C (002) with d-spacing of 3.37563°A (Fahem and Abbar, 2020). Scanning electron microscope (SEM, FEI-company) was used for testing the surface of GAC and both electrodes. Figure 3 illustrates SEM photos of GAC, copper foam and porous graphite before experiments. The SEM result of GAC shows a porous structure, while copper foam revealed a 3D network construction having a regular distribution of several interconnected pores. A great porosity with large pores shaped among interconnected structures can be showed by SEM images of porous graphite. The energy dispersive X-ray spectroscopy measurements (EDX, Bruker Company/Germany) with properties of 100 A, 25 kV and XFlash-6110 were depicted in Figure 4. This Figure illustrated that the main compositions of GAC, copper foam, and porous graphite were C, Cu, and C, respectively, with minor impurities.

Design of experiment

Design of experiment (DOE) and the optimization of variables were achieved by Box-Behnken design (BBD) by using Minitab-19. In this work, BBD based on 3 levels and 3 parameters which controlled the elimination of MO were utilized.

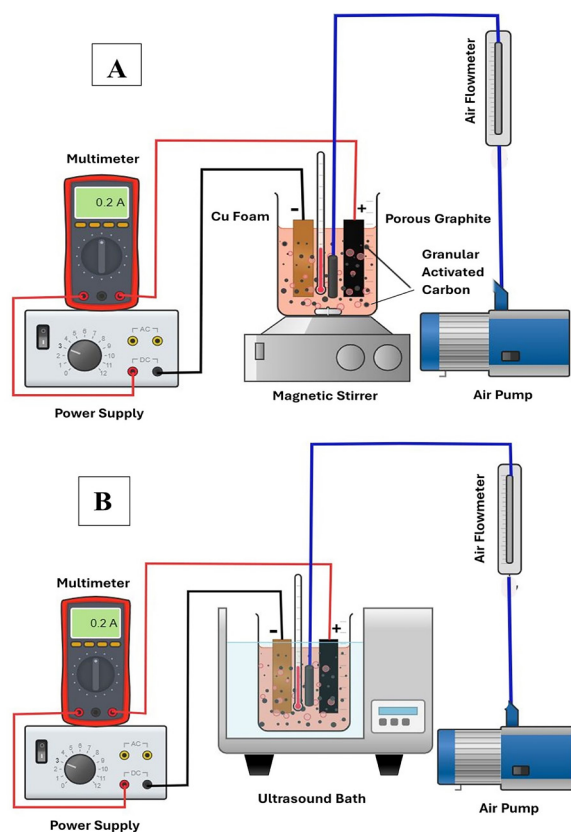


Figure 1. A schematic plot of (a) the 3D Electro Fenton and (b) the 3D Sono Electro Fenton systems

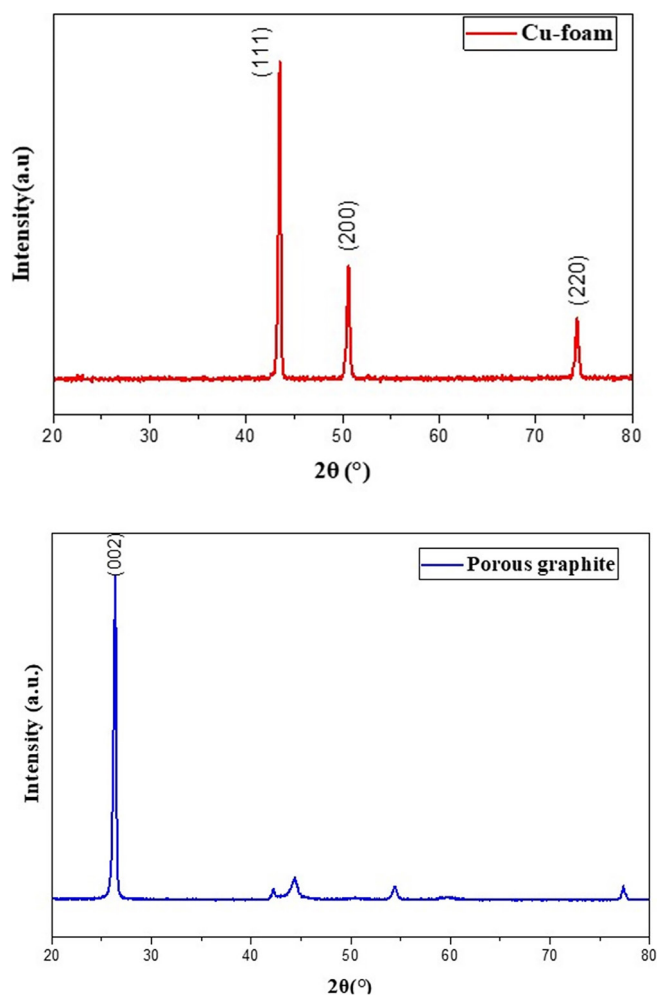


Figure 2. XRD for copper foam and porous graphite

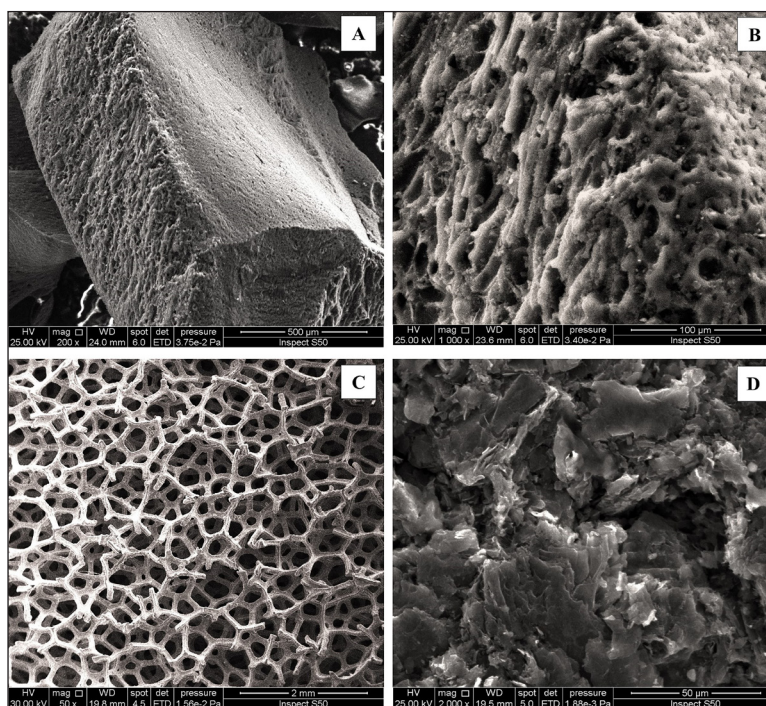


Figure 3. SEM of (a) GAC (with magnification of 500 μm), (b) GAC (with magnification of 100 μm), (c) copper foam (with magnification of 2 mm), and (d) porous graphite (with magnification of 50 μm)

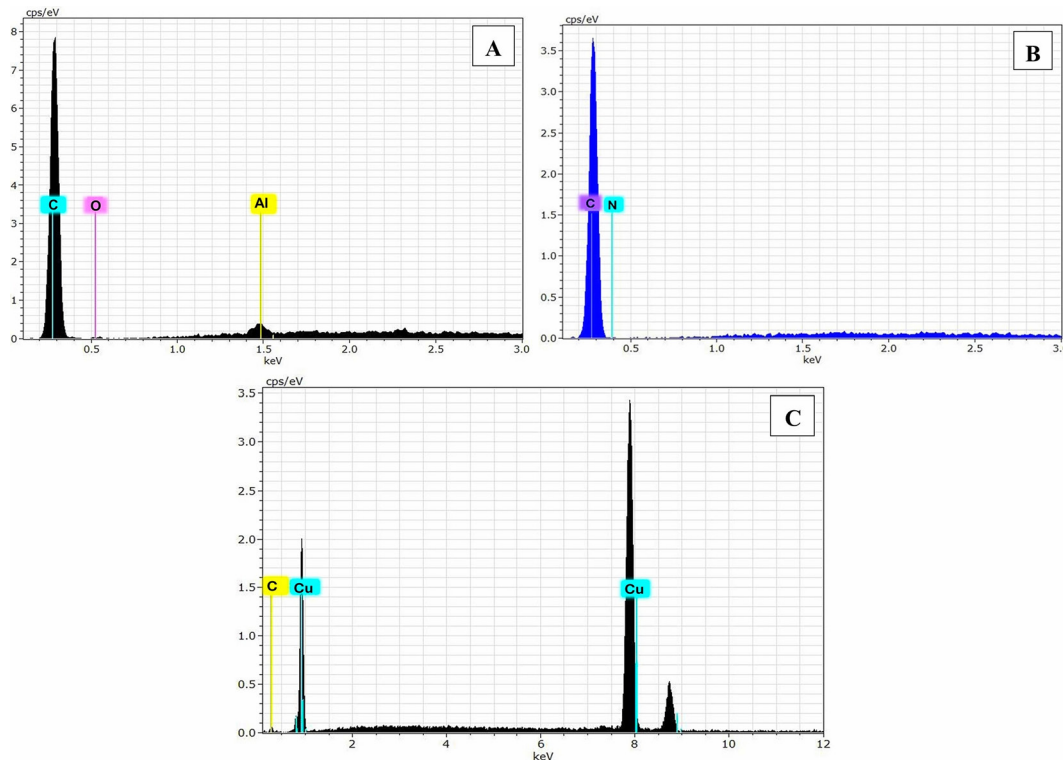


Figure 4. EDX of (a) GAC, (b) porous graphite, and (c) copper foam

The process factors were the current density (X1), GAC (X2) and time (X3), whereas the response was the MO removal efficiency (MO Re%). The process variables scales were represented to high level (+1), center point (0) and low level (-1). Minitab-19 was employed for testing the MO removal efficiency (Re%) outcomes. Table 2 exhibits the range of coded factors and their actual values, while Table 3 displays the runs based on BBD. The mathematical correlation between the parameters and the response can be represented by Equation 7, which represents the empirical quadratic polynomial model (Demirel et al., 2022).

$$Y = \gamma_0 + \sum \gamma_i x_i + \sum \gamma_{ii} x_i^2 + \sum \gamma_{ij} x_i x_j \quad (7)$$

where: *Y* is the predicted response (MO Re%), *k* is the numeral of the studied parameters, *x_i* and *x_j* are the coded process variables, γ_0 is the intercept, γ_i , γ_{ii} and γ_{ij} are the first- order main, the second- order main and the interaction effects, respectively (Demirel et al., 2022).

RESULTS AND DISCUSSION

Development of regression model and statistical analysis

Fifteen batch turns were carried out at various process parameters to be optimized and to investigate the combined influences of the studied variables on the MO Re%. Table 4 exhibits the experiment results of MO Re% with the predicted values of MO Re% based on Equation 8 with energy consumption values. Minitab-19 was utilized to predict the mathematical model of MO Re%, as illustrated in Equation 8.

$$\begin{aligned} MO\ Re\% = & -93.0 + 22.70 X1 + 13.59 X2 + \\ & + 10.76 X3 - 0.618 (X1)^2 + 0.59(X2)^2 - \\ & - 0.1538 (X3)^2 - 1.202 (X1X2) - \\ & - 0.6398 (X1X3) - 0.398 (X2X3) \end{aligned} \quad (8)$$

The outcomes revealed that the range of the MO Re% was 54.8676 to 97.6057 % and the range

Table 2. The operational variables and their levels

| Independent variable | Sings | Unit | Low (-1) | Middle (0) | High (+1) |
|----------------------|-------|--------------------|----------|------------|-----------|
| Current density | X1 | mA/cm ² | 3 | 5.5 | 8 |
| GAC | X2 | g | 1 | 2 | 3 |
| Time | X3 | min | 10 | 15 | 20 |

Table 3. Box-Behnken design for MO elimination

| Run | Bk. | Coded value | | | Actual value | | |
|-----|-----|-------------|----|----|---|-------------|----------------|
| | | X1 | X2 | X3 | Current density (mA/cm ²), X1 | GAC (g), X2 | Time (min), X3 |
| 1 | 1 | -1 | 1 | 0 | 3.0 | 3 | 15 |
| 2 | 1 | 1 | 1 | 0 | 8.0 | 3 | 15 |
| 3 | 1 | -1 | 0 | -1 | 3.0 | 2 | 10 |
| 4 | 1 | 0 | 0 | 0 | 5.5 | 2 | 15 |
| 5 | 1 | 1 | -1 | 0 | 8.0 | 1 | 15 |
| 6 | 1 | 1 | 0 | -1 | 8.0 | 2 | 10 |
| 7 | 1 | 0 | -1 | -1 | 5.5 | 1 | 10 |
| 8 | 1 | -1 | -1 | 0 | 3.0 | 1 | 15 |
| 9 | 1 | 0 | 1 | 1 | 5.5 | 3 | 20 |
| 10 | 1 | -1 | 0 | 1 | 3.0 | 2 | 20 |
| 11 | 1 | 0 | 0 | 0 | 5.5 | 2 | 15 |
| 12 | 1 | 1 | 0 | 1 | 8.0 | 2 | 20 |
| 13 | 1 | 0 | 1 | -1 | 5.5 | 3 | 10 |
| 14 | 1 | 0 | 0 | 0 | 5.5 | 2 | 15 |
| 15 | 1 | 0 | -1 | 1 | 5.5 | 1 | 20 |

Table 4. The experimental results for the removing of MO by employing Box-Behnken design, predicted values of MO Re%, and consumed energy

| Run | Current density (mA/cm ²) | GAC (g) | Time (min) | Actual MO Re% | Predicted MO Re% | E (Volt) | EC (kWh/kg MO) |
|-----|---------------------------------------|---------|------------|---------------|------------------|----------|----------------|
| 1 | 3.0 | 3 | 15 | 86.6964 | 84.9184 | 3 | 1.6105 |
| 2 | 8.0 | 3 | 15 | 97.6057 | 98.4361 | 6.3 | 8.6949 |
| 3 | 3.0 | 2 | 10 | 54.8676 | 56.9577 | 3.1 | 2.0108 |
| 4 | 5.5 | 2 | 15 | 91.9872 | 91.5699 | 5.2 | 4.7221 |
| 5 | 8.0 | 1 | 15 | 95.9104 | 97.6884 | 6.5 | 13.5802 |
| 6 | 8.0 | 2 | 10 | 92.9966 | 92.4783 | 6.3 | 5.7157 |
| 7 | 5.5 | 1 | 10 | 75.0619 | 73.8021 | 5.2 | 3.7242 |
| 8 | 3.0 | 1 | 15 | 72.9839 | 72.1535 | 3.4 | 2.5701 |
| 9 | 5.5 | 3 | 20 | 97.5898 | 98.8496 | 4.9 | 5.2240 |
| 10 | 3.0 | 2 | 20 | 90.7250 | 91.2433 | 3.1 | 2.4321 |
| 11 | 5.5 | 2 | 15 | 91.5699 | 91.5699 | 5.2 | 4.7804 |
| 12 | 8.0 | 2 | 20 | 96.8654 | 94.7753 | 6.3 | 10.9748 |
| 13 | 5.5 | 3 | 10 | 84.8503 | 84.5382 | 5 | 3.0655 |
| 14 | 5.5 | 2 | 15 | 91.1526 | 91.5699 | 5.2 | 6.0341 |
| 15 | 5.5 | 1 | 20 | 95.7611 | 96.0732 | 5.3 | 5.9507 |

of the specific energy consumption was 1.6105 to 13.5802 kWh/kg MO. Current density (CD) has the greater impact on the elimination of MO, as it appears from the contrast of runs 3 and 6, where, at a fixed value of time (10 min) and GAC dosage (2 g), the MO Re% increased from 54.8676% to 92.9966% with a distinction of 38.129% when the current density increased from 3 to 8 mA/cm². Moreover, the increasing in CD from 3 to 8 mA/cm² resulting a rise in EC from 2.0108 to 5.7157 kWh/kg MO. As

it is obvious in the runs 3 and 10, the MO Re% increased from 54.8676 to 90.725%, making a noticeable difference of 35.8574% by rising the time from 10 to 20 min that led it to be the second impact on the removal of MO. Also, increasing time corresponding to a small rising in EC from 2.0108 to 2.432 kWh/kg MO. Finally, the MO Re% increased from 72.9839 to 86.6964% with a 13.713% variance was attained, when GAC dose raised from 1 to 3 g as seen in the runs 1 and 8, with

decreasing in EC from 2.5701 to 1.6105 kWh/kg MO when increasing GAC dosage from 1 to 3 g because it led to rise in the MO Re%.

Analysis of variance (ANOVA)

To detect how much the results of BDD were acceptable, ANOVA was employed. Also, it is an active way for optimizing and conception the system. The ANOVA statistical terms like the sequential sum of the square (Seq. SS), the adjusted sum of the square (Adj. SS) and the adjusted mean of the square (Adj. MS) with the contribution percentage for each variable (contr.%) and the degree of freedom (DF) (Jasim and Salman, 2024b) were reported in Table 5.

The model's significance and its variables can be estimated by Fisher value (F-value) and the probability value (P-value). If F-value > 4 that means the variance in the response can be clarified adequately by means of the regression equation and when P-value < 0.05 it indicates that the model has statistical meaning (Özyurt et al., 2017; Jasim and Salman, 2024b).

The outcomes in Table 5 showed that the model for MO removal extremely meaningful with F-value and P-value of 52.01 and 0.000, respectively, and the description of the degradation operation effectively can be predicted by

this model. The multiple correlation coefficient (R^2) was 0.9894 with well-match observed between adj. R^2 (0.9704) and pred. R^2 (0.8334). The highest effect on MO removal efficiency was by current density followed by electrolysis time with contr.% of 38.94% and 34.17%, respectively. In turn, GAC dosage has the lowest impact on MO removal efficiency with 4.66%.

Effect of studied factors on the removal of MO

To investigate the synergistic impacts of studied parameters and their influences on the response more extensively, by depending on RSM analysis, a 3D surface plots with 2D plots were utilized as illustrated in Figures 5–7.

From the 3D surface diagram in Figure 5, The effectiveness of MO removal was examined by changing the current density (3, 5 and 8 mA/cm²) and GAC dosage (1, 2 and 3 g) under constant electrolysis time of 15 min. It was clear that the MO Re% grew as CD increased from 3 to 8 mA/cm² due to the rise in electro-formation of H₂O₂ which leading to an increment in OH^{*} which enhanced the rate of oxidation of contaminants (Beqqal et al., 2017; Gökkuş et al., 2018). These findings are approved by the outcomes of other studies (Adachi et al., 2022; Ghanbari and Moradi, 2015). It can be revealed that even at low values of GAC

Table 5. Variance analysis for MO elimination

| Source | DF | Seq SS | Contr.% | Adj SS | Adj MS | F-Value | P-Value |
|------------------------------|--------|----------------|----------------------|---------|------------------------|---------|---------|
| Model | 9 | 1937.41 | 98.94% | 1937.41 | 215.268 | 52.01 | 0.000 |
| Linear | 3 | 1522.98 | 77.78% | 1522.98 | 507.662 | 122.66 | 0.000 |
| C.D(mA/cm ²), X1 | 1 | 762.55 | 38.94% | 762.55 | 762.553 | 184.25 | 0.000 |
| GAC(G), X2 | 1 | 91.29 | 4.66% | 91.29 | 91.293 | 22.06 | 0.005 |
| Time (min), X3 | 1 | 669.14 | 34.17% | 669.14 | 669.139 | 161.68 | 0.000 |
| Square | 3 | 106.67 | 5.45% | 106.67 | 35.556 | 8.59 | 0.020 |
| X1X1 | 1 | 49.17 | 2.51% | 55.06 | 55.056 | 13.30 | 0.015 |
| X2X2 | 1 | 2.92 | 0.15% | 1.29 | 1.288 | 0.31 | 0.601 |
| X3X3 | 1 | 54.58 | 2.79% | 54.58 | 54.581 | 13.19 | 0.015 |
| 2-way interaction | 3 | 307.76 | 15.72% | 307.76 | 102.587 | 24.79 | 0.002 |
| X1X2 | 1 | 36.10 | 1.84% | 36.10 | 36.103 | 8.72 | 0.032 |
| X1X3 | 1 | 255.82 | 13.06% | 255.82 | 255.818 | 61.81 | 0.001 |
| X2X3 | 1 | 15.84 | 0.81% | 15.84 | 15.839 | 3.83 | 0.108 |
| Error | 5 | 20.69 | 1.06% | 20.69 | 4.139 | | |
| Lack-of-fit | 3 | 20.35 | 1.04% | 20.35 | 6.782 | 38.95 | 0.025 |
| Pure error | 2 | 0.35 | 0.02% | 0.35 | 0.174 | – | – |
| Total | 14 | 1958.11 | 100.00% | – | – | – | – |
| Model summary | S | R ² | R ² (adj) | Press | R ² (pred.) | – | – |
| | 2.0343 | 98.94% | 97.04% | 326.307 | 83.34% | – | – |

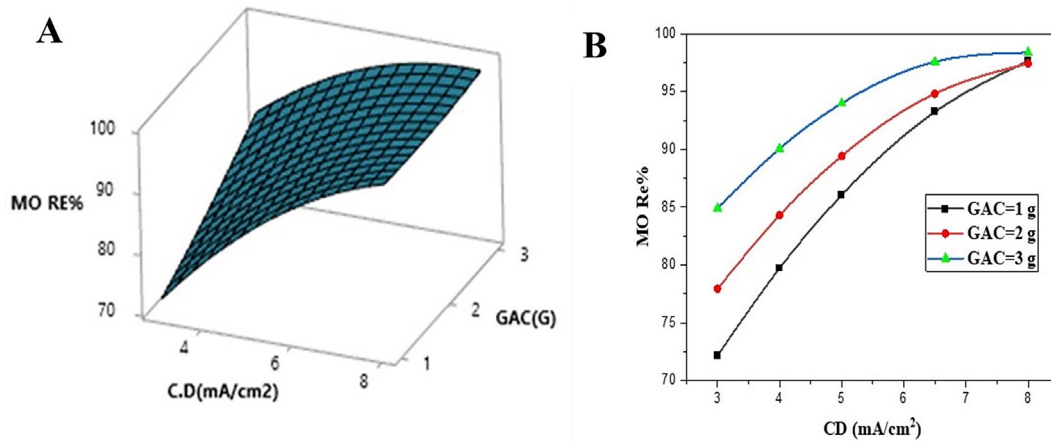


Figure 5. (a) 3D surface graph (b) 2D diagram for MO Re% at fixed Time of 15 min

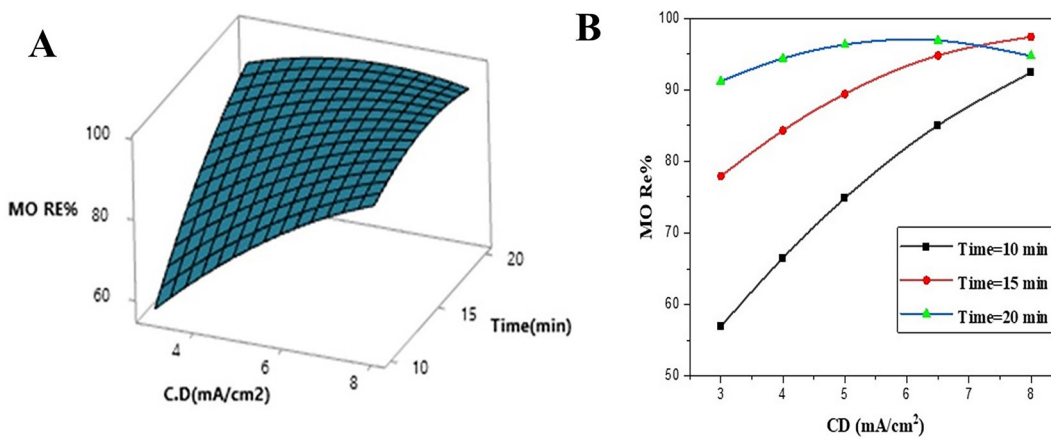


Figure 6. (a) 3D surface graph (b) 2D diagram for MO Re% at fixed GAC of 2 g

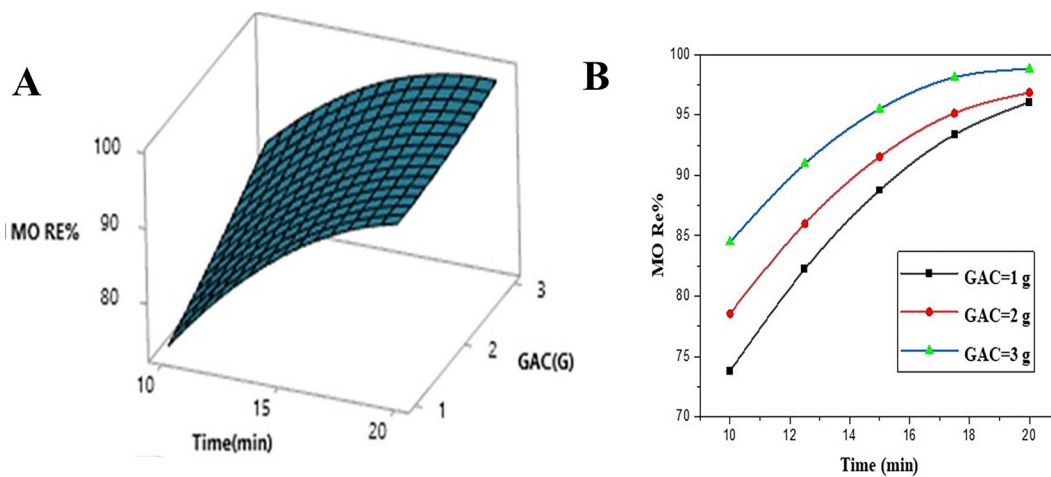


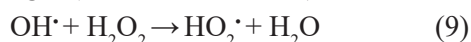
Figure 7. (a) 3D surface graph (b) 2D diagram for MO Re% at fixed CD of 5.5 mA/cm²

(1 g), the MO Re% was 95% at 8 mA/cm² which denotes the high impact of CD on the electro-Fenton system’s performance as revealed previously from ANOVA results. The type of material that used in the particles of the 3D electrode process

affects significantly the cost of system and its effectiveness (Yan et al., 2016). The use of the 3D electrochemical technique improved the rate of contaminants elimination due to their function as reactive sites for the absorption of contaminations

or as catalytic reactions caused by their high surface areas, in addition to being microelectrodes which reduce the concentration polarization (Dao et al., 2020). As shown in Figure 5B, the efficiency obviously increases along with the amount of GAC and its effect reduced with the rising of current density because the high values of current density were sufficient to achieve MO removal efficiency more than 95%.

Figure 6 demonstrates the impacts of CD and time on MO Re% at constant GAC dose of 2 g. The 3D surface diagram explains that the MO Re% is exponentially increased along with current density at a low value of time (10 min). However, there was no significant increment in MO Re% after 6 mA/cm², and the same pattern could be noticed as the time raised to 20 min, just with more dynamic behavior (Jiad and Abbar, 2023). As demonstrated in 2D plot (Figure 6B), MO Re% increased with time at low values of current density. This result can be attributed to the fact that high values of CD generate more hydrogen peroxide, thus increasing OH[•] as shown in Equation 1, then MO Re% increased, but this improvement becomes slight and even decreases with increasing time due to some side reactions. According to Equation 9, the excess H₂O₂ acts as OH[•] scavenger (He and Zhou, 2017).



At a fixed CD value of 5.5 mA/cm², Figure 7 depicts the interaction impacts of time and the amount of GAC. The degradation of MO increased exponentially with increasing time and linearly as the dosage of GAC increased. Electrolysis time is a fundamental operator as it effects the formation rate of OH[•] and decreasing organic contaminations. As it can be seen in Table 3 run 9, the MO removal efficiency was greater than 97% which achieved at 20 min and 3

g of GAC with constant CD of 5.5 mA/cm², so it is clearly that MO Re% rising at higher dosage of GAC with longer time (Thwaini and Salman, 2023).

Optimization and confirmation analysis

To achieve the lowest energy consumption for any electrochemical process, optimization of the system operating parameters is fundamental and must be attained by identified several criteria for improving the process to achieve the purpose goal through optimizing the desirability function (DF) by detecting the weight or importance (Chakawa and Aziz, 2021). There are five options available for the objective fields of parameters: maximize, objective, minimize, within the range and none. The target of MO elimination for EF process was specified as 'maximum' at DF = 1.0. The lower limit value of MO elimination was 54.86% while the upper limit was 97.6%, so the optimization process was performed according to these limits and variables, the results are displayed in Table 6. For obtaining the highest value of MO removal efficiency, two confirmation runs were accomplished according to the optimal settings for verifying them as illustrated in Table 7. Average MO Re% was 95.62% and it close to the lower limit of 95% CI because there was a disparity between R²(adj) and R²(pred.) less than 0.2 and greater than 0.1. However, it was acceptable as long as R² is closer to 1.

Performance of Sono-Electro-Fenton technique

For studying the improvement that can be obtained from the combination of EF with ultrasound (US), a new approach was adopted by determining the minimum conditions of EF before applying US. Table 8 showed the minimum

Table 6. Process variable optimization for optimal MO elimination efficiency

| Response | Goal | Lower | Target | Upper | Weight | Important |
|------------------------|--------|-----------|------------------------------|--------|----------------|----------------|
| Parameter | Max. | 54.86 | Max. | 97.60 | 1 | 1 |
| Solution of parameters | | | Multiple response prediction | | | |
| CD, mA/cm ² | GAC, g | Time, min | MO% fit | SE fit | 95% CI | 95% PI |
| 5.12121 | 3 | 20 | 98.9485 | 1.77 | (94.39,103.50) | (92.01,105.88) |

Table 7. The established result of optimum MO removal efficiency for maximum Electro-Fenton system

| Run | CD, mA/cm ² | GAC, g | Time, min | E, volt | EC, kWh/kg MO | Actual MO Re% | Average |
|-----|------------------------|--------|-----------|---------|---------------|---------------|---------|
| 1 | 5.12 | 3 | 20 | 4.9 | 6.3251 | 95.52 | 95.62 |
| 2 | 5.12 | 3 | 20 | 4.8 | 6.1148 | 95.72 | |

circumstances for EF by utilizing Minitab-19. To verify the accuracy of these conditions, two confirmatory experiments were accomplished, and the results shown in Table 9. The MO Re% as average value was 49.24% and it was within the range of the optimal value that estimated by Minitab-19, as displayed in Table 8. In the Sono Electro-Fenton (SEF) method, a slight enhancement in the elimination efficiency was attained by increasing it to 50.51%. The similar result was obtained by Şahinkaya (2013). The reason for this result might be the nature and the structure of the treated organic contaminant which is agreement with Oturan et al. (2008), they examined the influence of SEF on destroying of three kinds of organic contaminants: 2,4-dichlorophenoxyacetic acid (2,4-D), 4,6-dinitro-o-cresol (DNOC) and azobenzene (AB). They found that SEF significantly degrades each of 2,4-D and DNOC (herbicides), while it had almost no enhancement on the removal of AB dye. Therefore, the positive effect of US was not achieved because the EF alone with the copper foam as the cathode was efficient in accomplishing the quickest removal rate even at a short time and low current density (Table 10).

Comparison with previous studies

To emphasize the effectiveness of the copper foam electrode as a cathode for removing dyes within an electro-Fenton system, Table 11 illustrates a comparison between the current

study and other relevant studies that employing electro-Fenton method for degradation of dyes utilizing various kinds of cathode under different operational variables. It is easy to conclude that the copper foam electrode was superior to the rest of cathodes that were used in previous studies and this superiority could be perceived in the terms of the shorter reaction time and lower current density, in addition to lower consumption of chemicals like Na_2SO_4 and $[\text{Fe}^{2+}]$ without the addition of H_2O_2 , hence it is generated electrochemically, which makes this system economically efficient and environmentally friendly.

Copper foam analysis

A critical factor affecting the synthesis and formation of the Fenton reagent is the increase in surface area of the electrodes. The increase in of OH^\cdot formation could be achieved by promoting the specific surface area and conductivity of the cathode, leading to an enhancement in the elimination of organic contaminants (Ma et al., 2021). The 3D porous structure of pure copper foam can be seen through the SEM photo in Figure 3b. With copper foam, MO was efficiently eliminated, and the chemical reaction led to remarkable diminishing in the surface form. As it can be seen in Figure 8a, copper foam before reaction had a smooth surface, while Figure 8b illustrates the defects on the top of copper foam surface because it leached

Table 8. Process variable optimization for minimum MO elimination efficiency

| Response | Goal | Lower | Target | Upper | Weight | Important |
|------------------------|--------|-----------|------------------------------|--------|---------------|---------------|
| Re% | Min. | 54.86 | Min. | 97.60 | 1 | 1 |
| Solution of parameters | | | Multiple response prediction | | | |
| CD, mA/cm ² | GAC, g | Time, min | MO% fit | SE fit | 95% CI | 95% PI |
| 3 | 1 | 10 | 49.1761 | 2.40 | (43.00,55.35) | (41.08,57.27) |

Table 9. The established result of optimum MO removal efficiency for minimum Electro-Fenton system

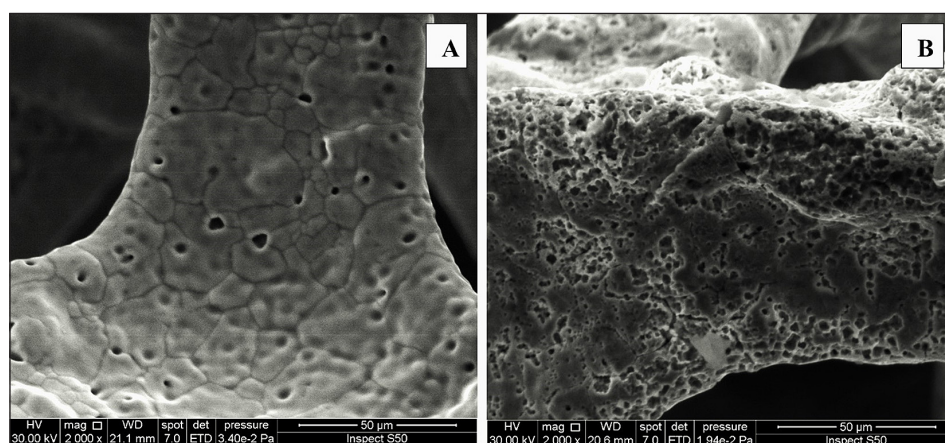
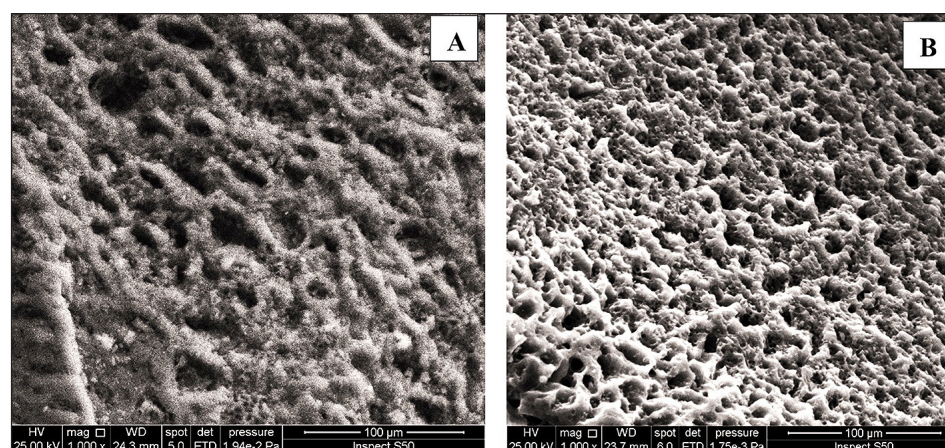
| Run | CD, mA/cm ² | GAC, g | Time, min | E, volt | EC, kWh/kg MO | Actual MO Re% | Average |
|-----|------------------------|--------|-----------|---------|---------------|---------------|---------|
| 1 | 3 | 1 | 10 | 3.3 | 2.3352 | 49.56 | 49.24 |
| 2 | 3 | 1 | 10 | 3.1 | 2.2033 | 48.92 | |

Table 10. The Sono-Electro-Fenton performance for minimum MO removal efficiency

| Run | CD, mA/cm ² | GAC, g | Time, min | E, volt | EC, kWh/kg MO | Actual MO Re% | Average |
|-----|------------------------|--------|-----------|---------|---------------|---------------|---------|
| 1 | 3 | 1 | 10 | 2.9 | 2.1151 | 50.30 | 50.51 |
| 2 | 3 | 1 | 10 | 2.9 | 2.0948 | 50.71 | |

Table 11. Comparison the results of current study with earlier researches

| Dye | Type of cathode | Optimal conditions | Re% | Reference |
|-----------------|-----------------|---|--------|-------------------------|
| MO | Graphite | [Fe ²⁺] = 2.14 mM, [Cl ⁻] = 16.36 mM, [Na ₂ SO ₄] = 0.05 M, pH = 3, Current = 2.1 A, time = 90 min, ambient temperature | 100% | (He et al., 2013) |
| Malachite green | Iron | pH = 3, CD = 10 mA/cm ² , [H ₂ O ₂] = 50 mg/l, time = 30 min, temperature = 50 °C | 99% | (Teimouri et al., 2018) |
| Remazol black B | Stainless steel | [Fe ²⁺]/[H ₂ O ₂] = 2 mM/750 ppm, pH = 3, CD = 10 mA/cm ² , time = 50 min | 95% | (Suhan et al., 2020) |
| MO | Graphite | [Fe ²⁺] = 0.232 mM, [H ₂ O ₂] = 8.8 mM, [Na ₂ SO ₄] = 0.05 M, pH = 3, Current = 80 mA, time = 60 min, temperature = 30 °C | 94.5% | (Adachi et al., 2022) |
| Red bemacid | Platinum grid | [Na ₂ SO ₄] = 0.09 M, pH = 2.8-3, Current I = 0.306 A, O ₂ sparging rate = 0.2 LPM, time = 60 min, ambient temperature | 94.51% | (Maamar et al., 2023) |
| MO | Copper foam | [Fe ²⁺] = 0.124 Mm, [Na ₂ SO ₄] = 0.02 M, pH = 3, CD = 5.12 mA/cm ² , air sparging rate = 18 L/h, time = 20 min, ambient temperature, GAC dose = 3g | 95.62% | Present study |

**Figure 8.** SEM image of copper foam (a) before reaction, and (b) after reaction, with magnification of 50 μm**Figure 9.** SEM image of GAC (a) before reaction, and (b) after reaction, with magnification of 100 μm

throughout the reaction, being symmetric with the upgraded degradation efficiency (Wan et al., 2017).

GAC analysis

Before reaction, the SEM photo of GAC was demonstrated in Figure 9A. GAC had a

great porosity with extensive pores established between the interconnected structures. GAC contains cavities that are important in adsorption process, as they allow the pollutant molecules to permeate the adsorbent (Thwaini and Salman, 2023; Trucillo et al., 2023). Figure 9 showed clearly the difference between the structure of GAC before and after reaction. It can be observed that the pores collapse, leading to their blockage and thus reducing the pore size from 0.2924 to 0.20104 cm³/g and surface area from 1023 to 752 m²/g at the end of reaction.

CONCLUSIONS

A 3D electro-Fenton system formed from the modifying of 2D electro-Fenton system by adding a certain amount of GAC was investigated to predict its improvement in the elimination of methyl orange. All studied parameters (current density, time of electrolysis, and GAC dose) influenced the MO removal efficiency which can be identified by the low P-values and high F-values. ANOVA evidenced that current density had the main influence on the MO Re% followed by time and GAC dosage. The high value of R² (0.9894) indicated that was a significant agreement between the model and the empirical data. The higher removal efficiency was 95.62% with energy consumption of 6.22 kWh/kg MO, which were achieved at 5.12 mA/cm² of CD, 3 g of GAC, and 20 min of electrolysis time, besides the fixed conditions (pH = 3, ambient temperature, and air flow = 18 L/h). Utilizing porous graphite as anode and copper foam as cathode enhanced the MO removal efficiency due to the large surface area of these electrodes. Under minimal circumstances (CD = 3 mA/cm², the mass of GAC = 1 g, and time = 10 min), the Re% for Sono electro-Fenton (SEF) was 50.51% with very low increasing in MO Re% if it was compared with the MO Re% for EF (49.24%) under the same conditions. This outcome resulted from the structure and the nature of the pollutant (MO) that might affect the performance of SEF. Finally, the system of 3D EF with cathode of copper foam and anode of porous graphite additional to GAC as third pole was an efficient method for wastewater treatment and gave a premium elimination of MO with lower energy exhaustion and lower quantities of added chemical components in comparison with previous studies.

REFERENCES

1. Najim, A.A., Mohammed, A.A. 2018. Biosorption of methylene blue from aqueous solution using mixed algae. *Iraqi Journal of Chemical and Petroleum Engineering*, 19(4), 1–11. <https://doi.org/10.31699/IJCPE.2018.4.1>
2. Abbas, R.N., Abbas, A.S. 2022. Kinetics and energetic parameters study of phenol removal from aqueous solution by electro-Fenton advanced oxidation using modified electrodes with PbO₂ and graphene. *Iraqi Journal of Chemical and Petroleum Engineering*, 23(2), 1–8. <https://doi.org/10.31699/IJCPE.2022.2.1>
3. Abed, I.A., Waisi, B.I. 2024. Performance enhancement of polyethersulfone-based ultrafiltration membrane decorated by titanium dioxide nanoparticles for dye filtration. *Ecological Engineering and Environmental Technology*, 25(5), 265–273. <https://doi.org/10.12912/27197050/186182>
4. Adachi, A., Ouadrhiri, F. El, Kara, M., El Manssouri, I., Assouguem, A., Almutairi, M.H., Bayram, R., Mohamed, H.R.H.H., Peluso, I., Eloutassi, N., Lahkimi, A., El Ouadrhiri, F., Kara, M., El Manssouri, I., Assouguem, A., Almutairi, M.H., Bayram, R., Mohamed, H.R.H.H., Peluso, I., Lahkimi, A. 2022. Decolorization and degradation of methyl orange azo dye in aqueous solution by the electro Fenton process: Application of optimization. *Catalysts*, 12(6), 665. <https://doi.org/10.3390/catal12060665>
5. Al-Bayati, I.S., Mohammed, S.A.M., Al-Anssari, S. 2023. Recovery of methyl orange from aqueous solutions by bulk liquid membrane process facilitated with anionic carrier. 060010. <https://doi.org/10.1063/5.0114631>
6. Babuponnusami, A., Muthukumar, K. 2014. A review on Fenton and improvements to the Fenton process for wastewater treatment. *Journal of Environmental Chemical Engineering*, 2(1), 557–572. <https://doi.org/10.1016/j.jece.2013.10.011>
7. Benmessaoud, S., Anissi, J., Kara, M., Assouguem, A., AL-Huqail, A.A., Germoush, M.O., Ullah, R., Ercisli, S., Bahhou, J. 2022. Isolation and characterization of three new crude oil degrading yeast strains, *Candida parapsilosis* SK1, *Rhodotorula mucilaginosa* SK2 and SK3. *Sustainability*, 14(6), 3465. <https://doi.org/10.3390/su14063465>
8. Beqqal, N., Yahya, M.S., EL Karbane, M., Guesous, A., El Kacemi, K. 2017. Kinetic study of the degradation/mineralization of aqueous solutions contaminated with Rosuvastatin drug by Electro-Fenton: Influence of experimental parameters. *Journal of Materials and Environmental Sciences*, 8(12), 4399–4407. <https://doi.org/10.26872/jmes.2017.8.12.464>
9. Chakawa, S., Aziz, M. 2021. Investigating the result of current density, temperature, and electrolyte

- concentration on COD: Subtraction of petroleum refinery wastewater using response surface methodology. *Water*, 13(6), 835. <https://doi.org/10.3390/w13060835>
10. Dao, K.C., Yang, C.-C., Chen, K.-F., Tsai, Y.-P. 2020. Recent trends in removal pharmaceuticals and personal care products by electrochemical oxidation and combined systems. *Water*, 12(4), 1043. <https://doi.org/10.3390/w12041043>
 11. Dargahi, A., Moradi, M., Marafat, R., Vosoughi, M., Mokhtari, S.A., Hasani, K., Asl, S.M. 2023. Applications of advanced oxidation processes (electro-Fenton and sono-electro-Fenton) for degradation of diazinon insecticide from aqueous solutions: optimization and modeling using RSM-CCD, influencing factors, evaluation of toxicity, and degradation pat. *Biomass Conversion and Biorefinery*, 13(12), 10615–10632. <https://doi.org/10.1007/s13399-021-01753-x>
 12. Demirel, C., Kabutey, A., Herák, D., Sedláček, A., Mizera, Č., Dajbych, O. 2022. Using box–Behnken design coupled with response surface methodology for optimizing rapeseed oil expression parameters under heating and freezing conditions. *Processes*, 10(3), 490. <https://doi.org/10.3390/pr10030490>
 13. Eslami, A., Khavari Kashani, M.R., Khodadadi, A., Varank, G., Kadier, A., Ma, P.-C., Madihi-Bidgoli, S., Ghanbari, F. 2021. Sono-peroxi-coagulation (SPC) as an effective treatment for pulp and paper wastewater: Focus on pH effect, biodegradability, and toxicity. *Journal of Water Process Engineering*, 44, 102330. <https://doi.org/10.1016/j.jwpe.2021.102330>
 14. Fahem, A.S., Abbar, A.H. 2020. Treatment of petroleum refinery wastewater by electro-Fenton process using porous graphite electrodes. *Egyptian Journal of Chemistry*, 63(12), 4805–4819. <https://doi.org/10.21608/EJCHEM.2020.28148.2592>
 15. Ganzenko, O., Oturan, N., Sirés, I., Huguenot, D., van Hullebusch, E. D., Esposito, G., Oturan, M.A. 2018. Fast and complete removal of the 5-fluorouracil drug from water by electro-Fenton oxidation. *Environmental Chemistry Letters*, 16(1), 281–286. <https://doi.org/10.1007/s10311-017-0659-6>
 16. Ghanbari, F., Moradi, M. 2015. A comparative study of electrocoagulation, electrochemical Fenton, electro-Fenton and peroxi-coagulation for decolorization of real textile wastewater: Electrical energy consumption and biodegradability improvement. *Journal of Environmental Chemical Engineering*, 3(1), 499–506. <https://doi.org/10.1016/j.jece.2014.12.018>
 17. Ghjeer, A.Y., Abbar, A.H. 2023. A comparative study of four technologies (Fenton, Sono-Fenton (SF), Electro-Fenton (EF), and Sono-Electro-Fenton (SEF)) for hospital wastewater treatment. *Case Studies in Chemical and Environmental Engineering*, 8(August), 100519. <https://doi.org/10.1016/j.cscee.2023.100519>
 18. Giray, S.N., Aktas, D., Dolaz, M., Uysal, Y. 2014. Removal of dye from real textile wastewater by Sono-Electro-Fenton oxidation process. *Journal of Selcuk University Natural and Applied Science*, May, 90–97.
 19. Gökkuş, Ö., Yıldız, N., Koparal, A.S., Yıldız, Y.Ş. 2018. Evaluation of the effect of oxygen on electro-Fenton treatment performance for real textile wastewater using the Taguchi approach. *International Journal of Environmental Science and Technology*, 15(2), 449–460. <https://doi.org/10.1007/s13762-017-1404-1>
 20. Hameed, M.F., Mousa, K.M. 2019. Study on kinetic and optimization of continuous advanced oxidative decolorization of brilliant reactive red dye. *Iraqi Journal of Chemical and Petroleum Engineering*, 20(1), 9–14. <https://doi.org/10.31699/IJCPE.2019.1.2>
 21. Hasani, K., Peyghami, A., Moharrami, A., Vosoughi, M., Dargahi, A. 2020. The efficacy of sono-electro-Fenton process for removal of Cefixime antibiotic from aqueous solutions by response surface methodology (RSM) and evaluation of toxicity of effluent by microorganisms. *Arabian Journal of Chemistry*, 13(7), 6122–6139. <https://doi.org/10.1016/j.arabjc.2020.05.012>
 22. Hassan, A.K., Atiya, M.A., Mahmoud, Z.A. 2022. Photo-Fenton-like degradation of direct blue 15 using fixed bed reactor containing bimetallic nanoparticles: Effects and Box–Behnken optimization. *Environmental Technology & Innovation*, 28, 102907. <https://doi.org/10.1016/j.eti.2022.102907>
 23. He, H., Zhou, Z. 2017. Electro-Fenton process for water and wastewater treatment. *Critical Reviews in Environmental Science and Technology*, 47(21), 2100–2131. <https://doi.org/10.1080/10643389.2017.1405673>
 24. He, W., Yan, X., Ma, H., Yu, J., Wang, J., Huang, X. 2013. Degradation of methyl orange by electro-Fenton-like process in the presence of chloride ion. *Desalination and Water Treatment*, 51(34–36), 6562–6571. <https://doi.org/10.1080/19443994.2013.792133>
 25. Igwegbe, C.A., Onukwuli, O.D., Ighalo, J.O., Umembamalu, C.J. 2021. Electrocoagulation-flocculation of aquaculture effluent using hybrid iron and aluminium electrodes: A comparative study. *Chemical Engineering Journal Advances*, 6, 100107. <https://doi.org/10.1016/j.cej.2021.100107>
 26. Jasim, R.A., Salman, R.H. 2024a. Congo red removal from aqueous solution by electrocoagulation-electro-oxidation combined system with Al and Cu–Mn–Ni nano composite as efficient electrodes. *Case Studies in Chemical and Environmental Engineering*, 9(March). <https://doi.org/10.1016/j.cscee.2024.100747>
 27. Jasim, R.A., Salman, R.H. 2024b. Use of nano Co-Ni-Mn composite and aluminum for removal

- of artificial anionic dye congo red by combined system. *Ecological Engineering & Environmental Technology*, 25(7), 133–149. <https://doi.org/10.12912/27197050/188266>
28. Jiad, M.M., Abbar, A.H. 2023. Treatment of petroleum refinery wastewater by electro-fenton process using a low cost porous graphite air-diffusion cathode with a novel design. *Chemical Engineering Research and Design*, 193, 207–221. <https://doi.org/10.1016/j.cherd.2023.03.021>
 29. Ma, B., Lv, W., Li, J., Yang, C., Tang, Q., Wang, D. 2021. Promotion removal of aniline with electro-Fenton processes utilizing carbon nanotube 3D morphology modification of an Ag-loaded copper foam cathode. *Journal of Water Process Engineering*, 43, 102295. <https://doi.org/10.1016/j.jwpe.2021.102295>
 30. Maamar, K., Fares, C., Sameut Bouhaik, I., Mahmoudi, L., Muthanna, B.G.N., Douani, M. 2023. Response surface methodology applied to Electro-Fenton process for degradation of red bemaicid as textile dye model. *Cellulose Chemistry And Technology*, 57(7–8), 891–901. <https://doi.org/10.35812/CelluloseChemTechnol.2023.57.78>
 31. Mohammed, M.A., Al-Bayati, I.S., Alobaidy, A.A., Waisi, B.I., Majeed, N. 2023. Investigation the efficiency of emulsion liquid membrane process for malachite green dye separation from water. *Desalination and Water Treatment*, 307(November), 190–195. <https://doi.org/10.5004/dwt.2023.29903>
 32. Mohammed, N.A., Alwared, A.I., Salman, M.S. 2020. Photocatalytic degradation of reactive yellow dye in wastewater using H₂O₂/TiO₂/UV technique. *Iraqi Journal of Chemical and Petroleum Engineering*, 21(1), 15–21. <https://doi.org/10.31699/IJCPE.2020.1.3>
 33. Norra, G.-F., Radjenovic, J. 2021. Removal of persistent organic contaminants from wastewater using a hybrid electrochemical-granular activated carbon (GAC) system. *Journal of Hazardous Materials*, 415, 125557. <https://doi.org/10.1016/j.jhazmat.2021.125557>
 34. Oturan, M.A., Sirés, I., Oturan, N., Pérocheau, S., Laborde, J.L., Trévin, S. 2008. Sono-electro-Fenton process: A novel hybrid technique for the destruction of organic pollutants in water. *Journal of Electroanalytical Chemistry*, 624(1–2), 329–332. <https://doi.org/10.1016/j.jelechem.2008.08.005>
 35. Özyurt, B., Camcioğlu, Ş., Hapoglu, H. 2017. A consecutive electrocoagulation and electro-oxidation treatment for pulp and paper mill wastewater. *Desalination and Water Treatment*, 93, 214–228. <https://doi.org/10.5004/dwt.2017.21257>
 36. Rivera, F.L., Menendez, N., Mazarío, E., Herrasti, P. 2022. Electro-fenton with reticular vitreous carbon and iron oxide nanoparticles for dye removal: A preliminary study. *Applied Sciences*, 12(16), 8293. <https://doi.org/10.3390/app12168293>
 37. Roddaeng, S., Promvong, P., Anuwattana, R. 2018. Behaviors of hydrogen sulfide removal using granular activated carbon and modified granular activated carbon. *MATEC Web of Conferences*, 192, 03037. <https://doi.org/10.1051/mateconf/201819203037>
 38. Şahinkaya, S. 2013. COD and color removal from synthetic textile wastewater by ultrasound assisted electro-Fenton oxidation process. *Journal of Industrial and Engineering Chemistry*, 19(2), 601–605. <https://doi.org/10.1016/j.jiec.2012.09.023>
 39. Sala, M., Gutiérrez-Bouzán, M.C. 2014. Electrochemical treatment of industrial wastewater and effluent reuse at laboratory and semi-industrial scale. *Journal of Cleaner Production*, 65, 458–464. <https://doi.org/10.1016/j.jclepro.2013.08.006>
 40. Staddon, C. 2016. *Managing Europe's water resources*. Routledge. <https://doi.org/10.4324/9781315593548>
 41. Suhan, M.B.K., Shuchi, S.B., Anis, A., Haque, Z., Islam, M.S. 2020. Comparative degradation study of remazol black B dye using electro-coagulation and electro-Fenton process: Kinetics and cost analysis. *Environmental Nanotechnology, Monitoring & Management*, 14, 100335. <https://doi.org/10.1016/j.enmm.2020.100335>
 42. Sun, Y., Li, P., Zheng, H., Zhao, C., Xiao, X., Xu, Y., Sun, W., Wu, H., Ren, M. 2017. Electrochemical treatment of chloramphenicol using Ti-Sn/ γ -Al₂O₃ particle electrodes with a three-dimensional reactor. *Chemical Engineering Journal*, 308, 1233–1242. <https://doi.org/10.1016/j.cej.2016.10.072>
 43. Teimouri, M., Khorsandi, H., Aghapour, A.A., Jafari, S.J. 2018. Degradation and mineralization of malachite green dye in aqueous solution by Electro-Fenton process using iron electrodes. *International Journal of Health and Life Sciences*, 4(1). <https://doi.org/10.5812/ijhls.79605>
 44. Tetteh, E.K., Obotey Ezugbe, E., Rathilal, S., Asante-Sackey, D. 2020. Removal of COD and SO₄²⁻ from oil refinery wastewater using a photo-catalytic system—Comparing TiO₂ and zeolite efficiencies. *Water*, 12(1), 214. <https://doi.org/10.3390/w12010214>
 45. Thwaini, H.H., Salman, R.H. 2023. Modification of Electro-Fenton Process with granular activated carbon for phenol degradation – Optimization by response surface methodology. *Journal of Ecological Engineering*, 24(9), 92–104. <https://doi.org/10.12911/22998993/168411>
 46. Trucillo, P., Lancia, A., Di Natale, F. 2023. Adsorption–Desorption process to separate dyes from tanning wastewaters. *Processes*, 11(10), 3006. <https://doi.org/10.3390/pr11103006>
 47. Vainoris, M., Nicolenco, A., Tsyntsar, N., Podlaha-Murphy, E., Alcaide, F., Cesiulis, H. 2022. Electro-deposited Fe on Cu foam as advanced fenton reagent

- for catalytic mineralization of methyl orange. *Frontiers in Chemistry*, 10. <https://doi.org/10.3389/fchem.2022.977980>
48. Wan, W., Zhang, Y., Ji, R., Wang, B., He, F. 2017. Metal foam-based Fenton-like process by aeration. *ACS Omega*, 2(9), 6104–6111. <https://doi.org/10.1021/acsomega.7b00977>
49. Yan, L., Wang, Y., Li, J., Shen, H., Zhang, C., Qu, T. 2016. Reduction of chemical oxygen demand from refinery wastewater by three-dimensional electrode-electro-fenton process. *Bulletin of the Chemical Society of Japan*, 89(1), 50–57. <https://doi.org/10.1246/bcsj.20150250>
50. Yang, B., Tang, J. 2018. Electrochemical oxidation treatment of wastewater using activated carbon electrode. *International Journal of Electrochemical Science*, 13(1), 1096–1104. <https://doi.org/10.20964/2018.01.78>
51. Yerima, E.A., Ogwuche, E., Ndubueze, C.I., Muhammed, K.A., Habila, J.D. 2024. Photocatalytic degradation of acid blue 25 dye in wastewater by zinc oxide nanoparticles. *Trends in Ecological and Indoor Environmental Engineering*, 2(1), 50–55. <https://doi.org/10.62622/TEIEE.024.2.1.50-55>
52. Zhang, M., Dong, H., Zhao, L., Wang, D., Meng, D. 2019. A review on Fenton process for organic wastewater treatment based on optimization perspective. *Science of The Total Environment*, 670, 110–121. <https://doi.org/10.1016/j.scitotenv.2019.03.180>
53. Zhang, Y., Chen, Z., Wu, P., Duan, Y., Zhou, L., Lai, Y., Wang, F., Li, S. 2020. Three-dimensional heterogeneous Electro-Fenton system with a novel catalytic particle electrode for Bisphenol A removal. *Journal of Hazardous Materials*, 393, 120448. <https://doi.org/10.1016/j.jhazmat.2019.03.067>
54. Zheng, Y., Qiu, S., Deng, F., Zhu, Y., Li, G., Ma, F. 2019. Three-dimensional electro-Fenton system with iron foam as particle electrode for folic acid wastewater pretreatment. *Separation and Purification Technology*, 224, 463–474. <https://doi.org/10.1016/j.seppur.2019.05.054>
55. Zhu, Y., Qiu, S., Deng, F., Ma, F., Li, G., Zheng, Y. 2020. Three-dimensional nickel foam electrode for efficient electro-Fenton in a novel reactor. *Environmental Technology*, 41(6), 730–740. <https://doi.org/10.1080/09593330.2018.1509890>